

Translationally invariant shell model calculation of the quasielastic $(p, 2p)$ process at intermediate relativistic energies

A.B. Larionov^{1a}, Yu.N. Uzikov^{2,3,4b}

¹ *Bogoliubov Laboratory of Theoretical Physics,
Joint Institute for Nuclear Research, 141980 Dubna, Russia*

² *Laboratory of Nuclear Problems, Joint Institute
for Nuclear Research, 141980 Dubna, Russia*

³ *Department of Physics, Moscow State University, 119991 Moscow, Russia*

⁴ *Dubna State University, 141980 Dubna, Russia*

Abstract

Relativistic beams of heavy ions interacting with various nuclear targets allow to study a broad range of problems starting from nuclear equation of state to the traditional nuclear structure. Some questions which were impossible to answer heretofore – can be addressed nowadays by using inverse kinematics. These includes the structure of short-lived nuclei and the precision study of exclusive channels with production of residual nuclei in certain quantum states. Theoretical understanding such processes is so far based on factorization models which combine the single-step amplitude of the reaction on a bound nucleon or nuclear cluster with a certain wave function of its relative motion with respect to the residual nucleus. The nuclear structure information is encoded in the spectroscopic amplitude, calculable within nuclear many-body theories. In this work, we use for this purpose the translationally-invariant shell model with configuration mixing and demonstrate that it successfully reproduces the single-differential and integrated cross sections of the quasielastic proton knockout, $^{12}\text{C}(p, 2p)^{11}\text{B}$, with outgoing ^{11}B in the ground state and low-lying excited states measured at GSI at 400 MeV/nucleon.

^a e-mail: larionov@theor.jinr.ru

^b e-mail: uzikov@jinr.ru

1. INTRODUCTION

Quasielastic (QE) knock-out reactions are the most direct way to access the momentum distribution of the valence nucleons given by the square of their wave function (WF) in momentum space. In the low-momentum region, the WFs are determined by nuclear mean field potential. Distortions of the incoming and outgoing proton waves including absorption effects are governed by nuclear optical potential that is mostly imaginary at high momenta and proportional to the local nuclear density. The nuclear mean field and optical potentials are rather well known for ordinary stable nuclei but represent a major uncertainty for exotic ones close to the neutron drip line. The studies of the structure of exotic nuclei using inverse kinematics with proton target at rest are in a focus of experiments at RIKEN [1] and GSI [2]. One of the most important questions is the quenching of single-particle strength and the dependence of this effect on the isospin asymmetry, see Ref. [3] for a recent review. As a first step, before being extended towards exotic nuclear region, any theoretical model of (p, pN) reactions should be tested for β -stable nuclear beams where a number of uncertainties in the model parameters is minimal.

In this work, we address the proton knock-out reaction $^{12}\text{C}(p, 2p)^{11}\text{B}$ measured in Ref. [4] with 400 MeV/nucleon ^{12}C beam colliding with proton target. We apply the translationally-invariant shell model (TISM) [5] which allows to calculate the spectroscopic amplitudes of the virtual decay $^{12}\text{C} \rightarrow p^{11}\text{B}$ for the given relative WF of the proton and residual nucleus and internal state of the residual nucleus. The present study is complementary to our previous work [6] where the TISM has been used to analyse the proton knock-out from a short-range correlated pN pair in the ^{12}C nucleus by a proton that yielded a good agreement with the BM@N data [7].

In sec. 2, the basic elements of our model are described starting from the amplitude in the impulse approximation (IA) and then adding the initial- and final state interactions (ISI/FSI) in the eikonal approximation. Explicit expression for the spectroscopic factor is derived from the TISM in the harmonic oscillator (HO) basis. Configuration mixing is accounted for within the intermediate coupling model [8, 9]. Sec. 3 contains results of our calculations of $^{12}\text{C}(p, 2p)^{11}\text{B}$ process at 400 MeV/nucleon in comparison with experimental data [4]. In sec. 4, we discuss various calculations of the spectroscopic factor and other sources of theoretical uncertainties. Sec. 5 summarizes the main results of the present work.

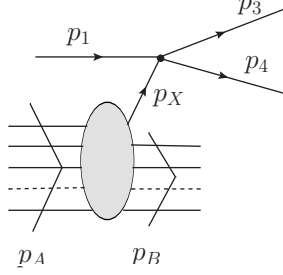


FIG. 1. The amplitude of the process $A(p, 2p)B$. The lines are marked with four-momenta of the particles: the initial (p_A) and final (p_B) nuclei, incident proton (p_1), struck proton (p_X), outgoing protons (p_3 and p_4).

2. THE MODEL

In the Feynman diagram representation, the amplitude of the studied process is shown in Fig. 1 which gives the following invariant matrix element:

$$M = M_{\text{el}}(p_3, p_4, p_1) \frac{i\Gamma_{A \rightarrow XB}(p_A, p_B)}{p_X^2 - m^2 + i\epsilon}, \quad (1)$$

where $M_{\text{el}}(p_3, p_4, p_1)$ is the invariant matrix element of elastic pp scattering amplitude, $\Gamma_{A \rightarrow XB}(p_A, p_B)$ is the nuclear virtual decay vertex, and m is the nucleon mass. The sum over all intermediate state quantum numbers is implicitly assumed in Eq.(1). For the residual nucleus B on the mass shell, in the rest frame (r.f) of the initial nucleus A , the decay vertex can be expressed as follows:

$$\frac{i\Gamma_{A \rightarrow XB}(p_A, p_B)}{p_X^2 - m^2 + i\epsilon} = S_A^X \left(\frac{2E_B m_A}{p_X^0} \right)^{1/2} (2\pi)^{3/2} \psi_{nl}^{m_l}(-\mathbf{p}_X), \quad (2)$$

where $\psi_{nl}^{m_l}(-\mathbf{p}_X)$ is the WF of the relative motion of the struck proton X and the nucleus B in momentum space with n being the HO main quantum number, l – the relative orbital momentum, and m_l – the magnetic quantum number. The WF is normalized as follows:

$$\int d^3 p_X |\psi_{nl}^{m_l}(-\mathbf{p}_X)|^2 = 1. \quad (3)$$

S_A^X is the spectroscopic amplitude, i.e. the virtual decay amplitude $A \rightarrow XB$ expressed via the overlap integral of the WF of the nucleus A and the antisymmetrized product of the

WF of the nucleus B and the relative WF of the proton X and nucleus B [10, 11]:

$$\begin{aligned}
S_A^X([f]LSTJMM_T; [f_B]L_B S_B T_B J_B M_B M_{T_B}; m_l, \sigma) &= A^{1/2} \langle \Psi_A | \Psi_B, nl \rangle \\
&= A^{1/2} \sum_{J_0 M_0} \left\{ \begin{array}{ccc} L_B & S_B & J_B \\ l & 1/2 & J_0 \\ L & S & J \end{array} \right\} \sqrt{(2L+1)(2S+1)(2J_B+1)(2J_0+1)} \\
&\quad \times \langle AN[f]LST | (A-1)N_B [f_B]L_B S_B T_B; nl \rangle \\
&\quad \times (J_B M_B J_0 M_0 | JM) (lm_l \frac{1}{2} \sigma | J_0 M_0) (T_B M_{T_B} \frac{1}{2} \tau | T M_T) , \tag{4}
\end{aligned}$$

where the internal WF of the initial nucleus $|\Psi_A\rangle \equiv |AN[f]LSTJMM_T\rangle$ is determined by N – the number of the oscillator quanta, $[f]$ – the Young scheme, L, S, J – the orbital, spin, and total angular momenta, respectively, T – isospin, M and M_T – z -components of J and T , respectively. The internal WF of the final nucleus is determined by similar quantum numbers $|\Psi_B\rangle \equiv |(A-1)N_B [f_B]L_B S_B T_B J_B M_B M_{T_B}\rangle$. The state of the struck nucleon X is determined by the spin, σ , and isospin, τ , projections. The numbers of oscillator quanta satisfy the sum rule $N = N_B + n$. For the WF of relative $X - B$ motion with quantum numbers $n = l = 1$, the one-particle fractional parentage coefficient (FPC) of the TISM (the term in the angular brackets in Eq.(4)) can be expressed via the FPC of the conventional shell model as follows [10]:

$$\begin{aligned}
&\langle AN[f]LST | (A-1)N_B [f_B]L_B S_B T_B; 11 \rangle \\
&= - \left(\frac{A-4}{A-1} \right)^{1/2} \langle p^{A-4} [f]LST | p^{A-5} [f_B]L_B S_B T_B \rangle . \tag{5}
\end{aligned}$$

The FPC of the conventional shell model can be calculated in a standard way from the tables of Ref. [12] taking into account the correction of phases of some orbital WFs as mentioned in the footnote of Ref. [13].

Equation (2) assumes transition from a TISM state of the nucleus A to a TISM state of the nucleus B . Eigenstates of a realistic nuclear Hamiltonian should be the superposition of TISM states. This means that actual spectroscopic amplitude for the transition between the physical states of the nuclei A and B is obtained by the weighted sum

$$\sum_{i,j} \alpha_i \beta_j^* S_A^X([f_i]L_i S_i T_i J_i M_i M_{T_i}; [f_j]L_j S_j T_j J_B M_B M_{T_B}; m_l, \sigma) \equiv S_A^X(J_i M_i M_{T_i}; J_B M_B M_{T_B}; m_l, \sigma) , \tag{6}$$

where the indices i and j enumerate the TISM states which enter the decomposition of the physical states of the nuclei A and B , respectively. The corresponding partial amplitudes α_i and β_j are model dependent. We will apply the intermediate coupling model of Ref. [9] which produces the real-valued partial amplitudes listed for ^{12}C ground state in Table I, and for ^{11}B ground state and two excited states in Table II.

TABLE I. Contributing $(1p)^8$ TISM states denoted as $[f]^{(2T+1)(2S+1)L}$ with their partial amplitudes for the ^{12}C ground state ($J = T = 0$). Taken from Ref. [9].

$[44]^{11}S$	$[431]^{13}P$	$[422]^{11}S$	$[422]^{15}D$	$[332]^{13}P$
0.840	0.492	0.064	-0.200	0.086

So far we discussed the case of IA neglecting ISI/FSI. We will now include the ISI/FSI in the eikonal approximation, similar to Ref. [6]. This is reached by replacing in Eq. (2)

$$(2\pi)^{3/2}\psi_{nl}^{m_l}(-\mathbf{p}_X) \rightarrow \int d^3r e^{-i\mathbf{p}_X\mathbf{r}} \psi_{nl}^{m_l}(-\mathbf{r}) F_1(\mathbf{r}) F_3(\mathbf{r}) F_4(\mathbf{r}) \equiv (2\pi)^{3/2} \tilde{\psi}_{nl}^{m_l}(-\mathbf{p}_X), \quad (7)$$

where $\mathbf{r} = \mathbf{R}_X - \mathbf{R}_B$ is the relative position vector of the struck proton and the center-of-mass (c.m.) of the residual nucleus B . Thus, Eq.(7) takes into account nuclear absorption introduced via factors

$$F_j(\mathbf{r}) = \exp\left(-\frac{i}{v_j} \int_{-\infty}^0 d\eta U_j(\mathbf{r} \pm \hat{\mathbf{p}}_j \eta)\right), \quad (8)$$

where $v_j = p_j/E_j$ is the j -th particle velocity in the rest frame (r.f.) of the nucleus B , $\hat{\mathbf{p}}_j \equiv \mathbf{p}_j/p_j$, and $U_j(\mathbf{r})$ is the optical potential. In Eq.(8), the integral is taken along the trajectory of the j -th particle that corresponds to the “+” sign for $j = 1$ (incoming proton) and “-” sign for $j = 3, 4$ (outgoing protons). At relativistic energies, in good approximation, the latter can be expressed as follows:

$$U_j(\mathbf{r}) = -\frac{i}{2} v_j \sigma_{NN}(p_j) \rho(\mathbf{r}), \quad (9)$$

where $\sigma_{NN}(p_j)$ is the total NN cross section, and $\rho(\mathbf{r})$ is the nucleon number density of the nucleus B in the point \mathbf{r} . The resulting absorption factors are then essentially similar to those in the Glauber approximation [14].

TABLE II. Same as in Table I but for $(1p)^7$ TISM states in ^{11}B . The ground state and two excited states are included. The values of excitation energy are experimental ones. Taken from Ref. [9].

$E^* = 0 \text{ MeV}, T = 1/2, J = 3/2$							
$[43]^{22}P$	$[43]^{22}D$	$[421]^{22}P$	$[421]^{24}P$	$[421]^{22}D$	$[421]^{24}D$	$[421]^{24}F$	
0.636	0.566	-0.223	-0.168	-0.087	-0.309	0.198	
$[331]^{24}S$	$[331]^{22}D$	$[331]^{24}D$	$[322]^{22}P$	$[322]^{24}P$	$[322]^{26}P$		
0.158	0.123	0.043	-0.016	0.080	0.080		

$E^* = 2.13 \text{ MeV}, T = 1/2, J = 1/2$							
$[43]^{22}P$	$[421]^{22}P$	$[421]^{24}P$	$[421]^{24}D$	$[331]^{22}S$	$[331]^{24}D$	$[322]^{22}P$	$[322]^{24}P$
0.913	0.161	-0.132	-0.314	0.126	-0.088	0.000	0.001

$E^* = 5.02 \text{ MeV}, T = 1/2, J = 3/2$						
$[43]^{22}P$	$[43]^{22}D$	$[421]^{22}P$	$[421]^{24}P$	$[421]^{22}D$	$[421]^{24}D$	$[421]^{24}F$
-0.532	0.721	-0.061	0.207	0.272	0.036	0.079
$[331]^{24}S$	$[331]^{22}D$	$[331]^{24}D$	$[322]^{22}P$	$[322]^{24}P$	$[322]^{26}P$	
-0.166	0.021	0.155	0.048	-0.039	-0.111	

We will consider the case of unpolarized particles and, thus, the matrix element modulus squared should be averaged over spin magnetic quantum numbers of the initial particles and summed over those of final particles:

$$\begin{aligned}
\overline{|M|^2} &\equiv \frac{1}{2(2J+1)} \sum_{\sigma_1, \sigma_3, \sigma_4, M, M_B} |M|^2 \\
&= \frac{1}{2(2J+1)} \sum_{\sigma_1, \sigma_3, \sigma_4, M, M_B} \sum_{\sigma, \sigma'} \sum_{m_l, m'_l} M_{\text{el}}(p_3, p_4, p_1; \sigma_3, \sigma_4, \sigma_1, \sigma) M_{\text{el}}^*(p_3, p_4, p_1; \sigma_3, \sigma_4, \sigma_1, \sigma') \\
&\quad \times \frac{2E_B m_A}{p_X^0} (2\pi)^3 \tilde{\psi}_{11}^{m_l}(-\mathbf{p}_X) \tilde{\psi}_{11}^{m'_l*}(-\mathbf{p}_X) \\
&\quad \times S_A^X(JMM_T; J_B M_B M_{T_B}; m_l, \sigma) S_A^{X*}(JMM_T; J_B M_B M_{T_B}; m'_l, \sigma'), \tag{10}
\end{aligned}$$

where we explicitly included summations over intermediate state quantum numbers $\sigma, \sigma', m_l, m'_l$.

To simplify Eq.(10), we, first, neglect the interference terms with $\sigma' \neq \sigma$ and replace

$$\begin{aligned} & \frac{1}{2} \sum_{\sigma_1, \sigma_3, \sigma_4} |M_{\text{el}}(p_3, p_4, p_1; \sigma_3, \sigma_4, \sigma_1, \sigma)|^2 \\ & \rightarrow \overline{|M_{\text{el}}(p_3, p_4, p_1)|^2} \equiv \frac{1}{4} \sum_{\sigma_1, \sigma_3, \sigma_4, \sigma} |M_{\text{el}}(p_3, p_4, p_1; \sigma_3, \sigma_4, \sigma_1, \sigma)|^2 . \end{aligned} \quad (11)$$

Then, after somewhat lengthy but straightforward derivation we come to the following expression:

$$\overline{|M|^2} = \overline{|M_{\text{el}}(p_3, p_4, p_1)|^2} \frac{2E_B m_A}{p_X^0} (2\pi)^3 \overline{|\tilde{\psi}_{11}(-\mathbf{p}_X)|^2} S , \quad (12)$$

where

$$\overline{|\tilde{\psi}_{11}(-\mathbf{p}_X)|^2} \equiv \frac{1}{3} \sum_{m_l=-1}^1 |\tilde{\psi}_{11}^{m_l}(-\mathbf{p}_X)|^2 . \quad (13)$$

The spectroscopic factor in Eq.(12) is expressed as follows:

$$\begin{aligned} S = & A (T_B M_{T_B} \frac{1}{2} \tau |T M_T|^2 (2J_B + 1) \sum_{J_0} (2J_0 + 1) \left| \sum_{i,j} \alpha_i \beta_j^* \begin{Bmatrix} L_j & S_j & J_B \\ 1 & 1/2 & J_0 \\ L_i & S_i & J \end{Bmatrix} \right| \\ & \times \sqrt{(2L_i + 1)(2S_i + 1)} \langle AN[f_i] L_i S_i T | (A - 1) N_B[f_j] L_j S_j T_B; 11 \rangle|^2 . \end{aligned} \quad (14)$$

Equation (13) for the modulus squared of the ISI/FSI-corrected WF is quite involved but can be simplified. Substituting Eq.(7) in Eq.(13) we have:

$$\begin{aligned} \overline{|\tilde{\psi}_{11}(-\mathbf{p}_X)|^2} &= \frac{1}{3(2\pi)^3} \sum_{m_l} \int d^3 r \int d^3 r' e^{-i\mathbf{p}_X(\mathbf{r}-\mathbf{r}')} \psi_{11}^{m_l}(-\mathbf{r}) \psi_{11}^{m_l*}(-\mathbf{r}') F_{\text{abs}}(\mathbf{r}) F_{\text{abs}}(\mathbf{r}') \\ &\simeq \frac{1}{(2\pi)^3} \int d^3 R f_{11}(-\mathbf{R}, -\mathbf{p}_X) F_{\text{abs}}^2(\mathbf{R}) , \end{aligned} \quad (15)$$

where $F_{\text{abs}}(\mathbf{r}) \equiv F_1(\mathbf{r}) F_3(\mathbf{r}) F_4(\mathbf{r})$ is the absorption factor, and

$$f_{11}(-\mathbf{R}, -\mathbf{p}_X) \equiv \frac{1}{3} \sum_{m_l} \int d^3 \xi e^{-i\mathbf{p}_X \xi} \psi_{11}^{m_l}(-\mathbf{R} - \xi/2) \psi_{11}^{m_l*}(-\mathbf{R} + \xi/2) \quad (16)$$

is a Wigner function. In Eq.(15), in the last step, we introduced variables $\mathbf{R} \equiv (\mathbf{r} + \mathbf{r}')/2$, $\xi \equiv \mathbf{r} - \mathbf{r}'$ and approximately set $\xi = 0$ in the product of absorption factors $F_{\text{abs}}(\mathbf{R} + \xi/2) F_{\text{abs}}(\mathbf{R} - \xi/2)$ (see Ref. [6] for discussion of validity of this approximation).

The TISM WF of the relative $X - B$ motion is

$$\psi_{11}^{m_l}(-\mathbf{R}) = \left(\frac{8}{3\pi^{1/2} R_0^5} \right)^{1/2} R e^{-R^2/2R_0^2} Y_{1m_l}(-\hat{\mathbf{R}}) , \quad (17)$$

where $R_0 = r_0[A/(A-1)]^{1/2}$, and $r_0 = 1.581$ fm is the parameter of the conventional HO shell model [15]. The Wigner function (16) can be then easily calculated:

$$f_{11}(-\mathbf{R}, -\mathbf{p}_X) = 8 e^{-(R^2 + p_X^2 R_0^4)/R_0^2} \left[\frac{2}{3R_0^2} (R^2 + p_X^2 R_0^4) - 1 \right]. \quad (18)$$

This expression can be used in Eq.(15) for numerical calculations of $|\overline{\psi_{11}(-\mathbf{p}_X)}|^2$ taking into account ISI/FSI. In the case of IA, one recovers an analytical formula:

$$|\overline{\psi_{11}(-\mathbf{p}_X)}|^2 = \frac{2R_0^5}{3\pi^{3/2}} p_X^2 e^{-p_X^2 R_0^2}. \quad (19)$$

The invariant matrix element of elastic pp scattering is related to the differential cross section by a standard formula:

$$\frac{d\sigma_{\text{el}}}{dt} = \frac{|M_{\text{el}}(t, s)|^2}{64\pi I_{pp}^2}, \quad (20)$$

where $I_{pp} = \sqrt{(s/4 - m^2)s}$ is the flux factor, $s = (p_3 + p_4)^2$, $t = \max\{(p_1 - p_3)^2, (p_1 - p_4)^2\}$. By using the high-energy parameterization $d\sigma_{\text{el}}/dt \propto e^{bt}$ one obtains the following relation:

$$|\overline{M_{\text{el}}(t, s)}|^2 = 64\pi I_{pp}^2 \frac{b\sigma_{\text{el}}}{1 - e^{bt_0}} e^{bt}, \quad (21)$$

where $t_0 = -2(s/4 - m^2)$. The experimental integrated elastic pp cross section, σ_{el} , and the slope parameter, b , are conveniently parameterized in Ref. [16] as functions of the beam momentum, $p_{\text{lab}} = I_{pp}/m$, for $p_{\text{lab}} \lesssim 5 - 6$ GeV/c.

For the calculation of the optical potential, Eq.(9), one has to specify the total pN cross section and the nucleon density distribution. We apply the proton/neutron-number-weighted formula

$$\sigma_{pN} = [\sigma_{pp}Z_B + \sigma_{pn}(A_B - Z_B)]/A_B, \quad (22)$$

where σ_{pp} and σ_{pn} are, respectively, the total pp and pn cross sections in the parameterizations of Ref. [16] that provide good fits of available experimental data at $p_{\text{lab}} \lesssim 3 - 5$ GeV/c. $A_B = A - 1$ and $Z_B = Z - 1$ are, respectively, the mass and charge numbers of the residual nucleus B . The nucleon density distribution in the nucleus with A_B nucleons in the $s^4 p^{A_B-4}$ configuration is described by the conventional HO shell model formula

$$\rho(r) = \frac{4}{r_0^3 \pi^{3/2}} \left[1 + \frac{A_B - 4}{6} \left(\frac{r}{r_0} \right)^2 \right] e^{-r^2/r_0^2}. \quad (23)$$

The fully differential cross section of the process $A(p, 2p)B$ (see Fig. 1 for notation) is expressed as follows:

$$d\sigma_{1A \rightarrow 34B} = \frac{(2\pi)^4 |\overline{M}|^2}{4I_{pA}} \delta^{(4)}(p_1 + p_A - p_3 - p_4 - p_B) \frac{d^3p_3}{(2\pi)^3 2E_3} \frac{d^3p_4}{(2\pi)^3 2E_4} \frac{d^3p_B}{(2\pi)^3 2E_B}, \quad (24)$$

where $I_{pA} = p_{\text{beam}}m$ is the flux factor, p_{beam} is the momentum of the nucleus A in the r.f. of the proton 1 which will be called ‘‘laboratory frame’’ below.. The experiment of Ref. [4] has been performed at $p_{\text{beam}}/A = 0.951$ GeV/c where the pp elastic cross section is almost isotropic in the effective region of integration over transferred rescattering momentum in the c.m. frame as follows from the used here parameterization [16].

Thus, it is convenient to perform the integration over invariants d^3p_3/E_3 and d^3p_4/E_4 in the c.m. frame of the protons 3 and 4. On the other hand, the matrix element is proportional to the WF of the relative $X - B$ motion which suppresses large absolute values of the momentum \mathbf{p}_B of the residual nucleus in the r.f. of the nucleus A . Thus, the integration over invariant d^3p_B/E_B is reasonable to perform in the r.f. of the nucleus A . As a result, we come to the following expression for the integrated cross section:

$$\sigma_{1A \rightarrow 34B} = \frac{1}{32(2\pi)^5 p_{\text{beam}}m} \int \frac{d^3p_B}{\sqrt{p_B^2 + m_B^2}} \int \frac{p_3 d\Omega_3}{2\sqrt{p_3^2 + m^2}} |\overline{M}|^2, \quad (25)$$

where the momentum \mathbf{p}_B is defined in the r.f. of the nucleus A while the momentum \mathbf{p}_3 and the corresponding solid angle element $d\Omega_3$ – in the c.m. frame of the protons 3 and 4. Due to identity of the differential cross section with respect to the interchange of momenta of the 3-d and 4-th protons, the integration over $d\Omega_3$ should be performed over the solid angle hemisphere of 2π (the orientation of the hemisphere does not play a role). Due to rotational symmetry about the beam axis, it is also possible to reduce the integration order by writing in the spherical coordinates with z -axis along the 1-st proton momentum in the r.f. of A $d^3p_B = p_B^2 dp_B 2\pi d\Theta_B$ and perform all integrations in Eq.(25) with arbitrarily fixed value of the azimuthal angle ϕ_B . Finally, the differential cross sections, $d\sigma_{1A \rightarrow 34B}/dx$, where x is any kinematic variable determined by the momenta \mathbf{p}_3 and \mathbf{p}_B , are evaluated by multiplying the integrand of Eq.(25) by the factor $\delta[x - x(\mathbf{p}_B, \mathbf{p}_3)]$.

3. RESULTS

The integrated cross sections are listed in Table III. One can see from this Table that absorption reduces all partial cross section by a factor of 5.1 but does not change the ra-

tios between the partial cross sections for different states of ^{11}B . The experimental total cross section is reproduced by full calculation surprisingly well, with accuracy of about 3%. The strong dominance of ^{11}B production in the ground state is also correctly reproduced. Discrepancies for excited states are quite large. However, this is still satisfactory given the fact that we did not introduce any additional model parameters (like phenomenological spectroscopic factors, see discussion section) to tune our calculations.

TABLE III. Integrated cross sections of the process $^{12}\text{C}(p, 2p)^{11}\text{B}$ with 400 MeV/nucleon ^{12}C beam for the ground state and two excited states of the residual nucleus ^{11}B . Listed are the results of full calculations (including absorption), calculations in the IA, and the spectroscopic factors calculated using Eq.(14). Experimental data are from Ref. [4]. Total errors are given in parentheses.

E^* (MeV)	J^π	σ_{exp} (mb)	σ_{full} (mb)	σ_{IA} (mb)	S
0.0 (G.S.)	$3/2^-$	15.8(18)	12.3	62.6	2.82
2.13	$1/2^-$	1.9(2)	2.9	14.9	0.67
5.02	$3/2^-$	1.5(2)	3.4	17.5	0.79
Total:		19.2(3)	18.6	95.0	4.28

Fig. 2 shows the distribution of opening angle, $\Theta_{\text{opening}} = \arccos(\mathbf{p}_3\mathbf{p}_4/p_3p_4)$, between outgoing protons in the laboratory frame. The full calculation correctly describes the peak position at 80° and the distribution at smaller angles, although gives a sharper peak and steeper fall-off at larger angles. The full calculation is slightly shifted to larger opening angles as compared to the calculation in the IA.

Fig. 3 shows the distribution of relative azimuthal angle, $\Delta\phi = \arccos(\mathbf{p}_{3t}\mathbf{p}_{4t}/p_{3t}p_{4t})$, between the transverse momenta \mathbf{p}_{3t} and \mathbf{p}_{4t} of outgoing protons. The absorptive ISI/FSI suppress the yield at large deviations of $\Delta\phi$ from 180° leading to a sharper peak at $\Delta\phi = 180^\circ$ and better agreement with experiment.

Figs. 4,5 and 6 show, respectively, the transverse, longitudinal, and total momentum distributions of the residual nucleus. Absorption leads to the depletion of the yield at large transverse and total momenta shifting the maxima of the P_{tr} - and P_{tot} distributions to smaller momenta. This can be understood as follows. In the presence of absorption, the main contribution to the integral in Eq.(15) comes from nuclear periphery (surface ring), since

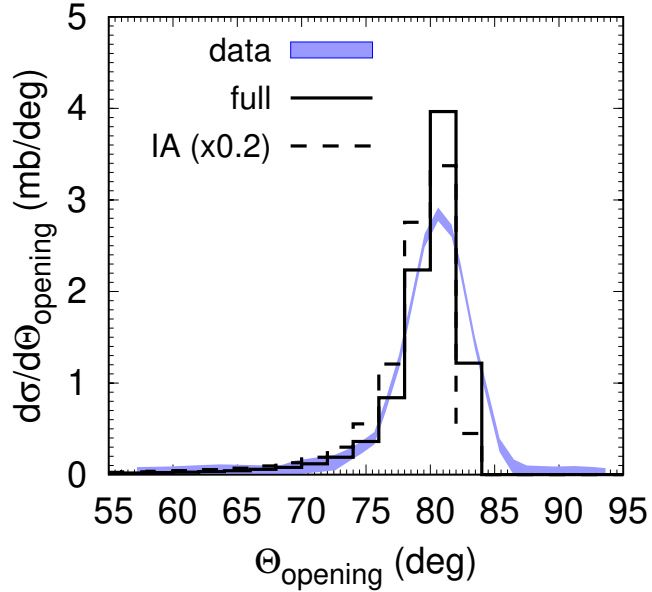


FIG. 2. The distribution of opening angle between outgoing protons in the laboratory frame for the process $^{12}\text{C}(p, 2p)^{11}\text{B}$ at 400 MeV/nucleon. Solid and dashed histograms show, respectively, the full calculation and the calculation without absorption scaled by a factor of 0.2. The band represents experimental data from Ref. [4].

the absorption factor suppresses the integrand deeply inside the nucleus. If the transverse momentum of the residual nucleus is small, then the absorption is in average smaller because both outgoing protons may have small transverse momenta balancing each other and their trajectories avoid the bulk of the nuclear medium. If the transverse momentum of the residual nucleus is large, then at least one of the outgoing protons will have large transverse momentum and, thus, its trajectory will pass through the bulk of the nuclear medium with a larger probability which makes absorption stronger. This is also in-line with stronger absorption at larger deviations of $\Delta\phi$ from 180° (Fig. 3).

A particular form of the Wigner density for the $n = l = 1$ valence nucleon, Eq.(18), acts in the same direction. At small values of R and $p_X (= P_{\text{tot}})$, the Wigner density becomes negative. It means that absorption should then lead to the enhancement of production which is visible at small values of P_{tot} in Fig. 6.

In the IA calculation, the longitudinal momentum distribution (Fig. 5) is shifted to positive P_{\parallel} . This corresponds to the struck proton X moving opposite to the incoming

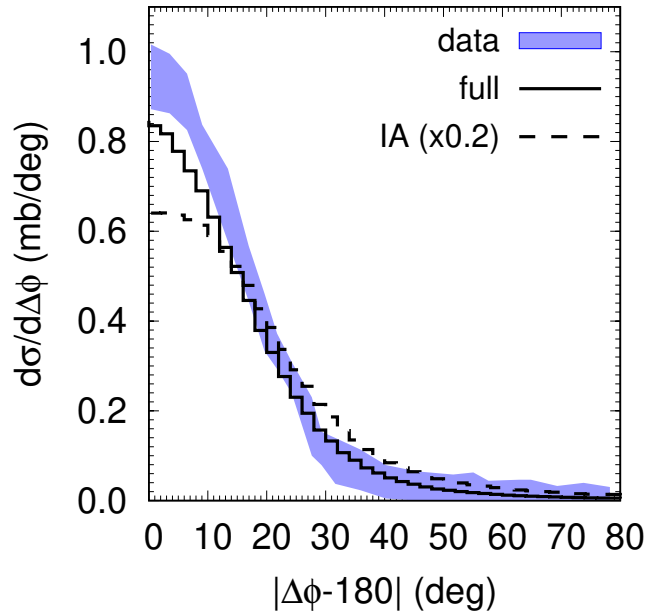


FIG. 3. The distribution of the relative azimuthal angle between transverse momenta of outgoing protons for $^{12}\text{C}(p, 2p)^{11}\text{B}$ at 400 MeV/nucleon. Line notations are the same as in Fig. 2. The band represents experimental data from Ref. [4].

proton 1 in the r.f. of ^{12}C giving a larger two-body phase space volume of the protons 3 and 4 (the term $\propto p_3/\sqrt{p_3^2 + m^2}$ in Eq.(25)). However, with absorption, the $P_{||}$ distribution becomes almost symmetric with respect to the change $P_{||} \rightarrow -P_{||}$. This is a consequence of larger average transverse momenta of the 3-d and 4-th protons at $P_{||} > 0$ leading to their stronger absorption. This observation also explains the stronger absorption at smaller opening angles (Fig. 2).

4. DISCUSSION

Table IV contains results of several other calculations of the spectroscopic factors for the separation of a nucleon from ^{12}C in comparison with our results. The approach of Ref. [17] is based on the FPCs of the conventional shell model but in other aspects is quite close to the intermediate coupling model of Refs. [8, 9] applied in our work. In Ref. [18], the WFs of deformed HO shell model were used without residual interaction taking $K = 0$ for ^{12}C and $K = 1/2, 3/2$ for ^{11}B . (In the spherical HO model this corresponds to considering

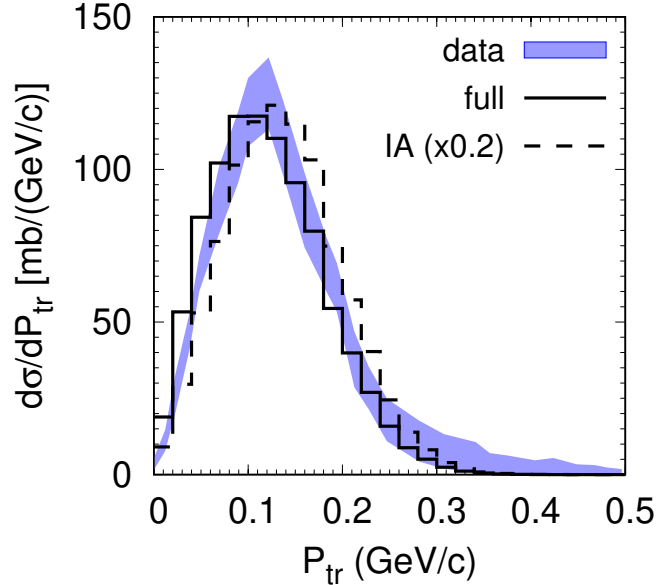


FIG. 4. The distribution of the transverse momentum of the residual nucleus for $^{12}\text{C}(p, 2p)^{11}\text{B}$ at 400 MeV/nucleon. Line notations are the same as in Fig. 2. The band represents experimental data from Ref. [4].

TABLE IV. Spectroscopic factors for the $^{12}\text{C} \rightarrow p^{11}\text{B}(n^{11}\text{C})$ process calculated in different theoretical models.

E^* (MeV)	J^π	[17]	[18]	[19]	this work
0.0 (G.S.)	$3/2^-$	2.85	3.27	2.50	2.82
2.13	$1/2^-$	0.75	0.60	0.48	0.67
5.02	$3/2^-$	0.38	0.12		0.79
Total:		3.98	3.99	2.98	4.28

only the Young scheme [44] for ^{12}C and [43] for ^{11}B .) In Ref. [19], the no-core shell model was employed in the HO basis with c.m. correction, although the authors state that the dependence of their results on the chosen basis is small. According to Ref. [20], however, the “old” definition of the spectroscopic amplitude (c.f. our Eq.(4)) relies on the non-normalized

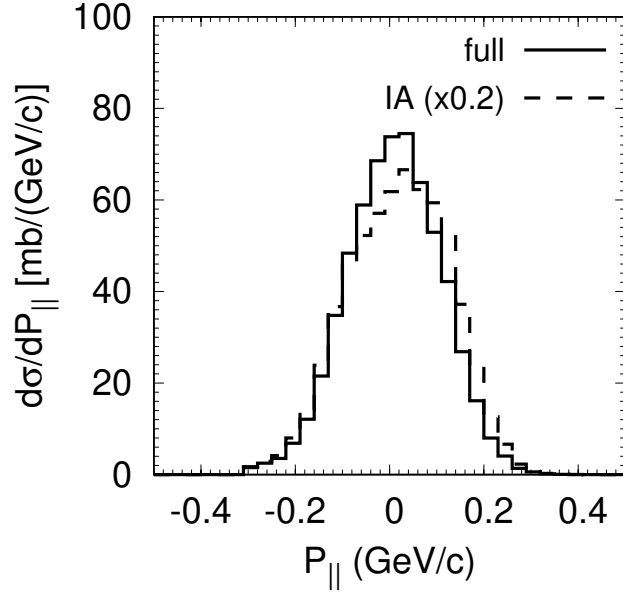


FIG. 5. The distribution of the longitudinal momentum of the residual nucleus in the r.f. of ^{12}C for $^{12}\text{C}(p, 2p)^{11}\text{B}$ at 400 MeV/nucleon. Positive values of $P_{||}$ correspond to the direction of the momentum of the incoming proton. Line notations are the same as in Fig. 2.

WF of the final state and, thus, should be corrected.¹

Comparison with experimental data for the QE (p, pN) processes depends not only on the spectroscopic factors but also on the ISI/FSI used. In phenomenological DWIA approaches [21, 22], the spectroscopic factor is used as a free parameter to fit experimental cross sections for some fixed ISI/FSI. The latter includes in-medium effects due to Pauli blocking of NN scattering [23] (i.e. the antisymmetrization of the full WF of the scattered nucleon and residual nucleus) which can be effectively described by in-medium reduced NN cross sections. It was shown [23], that in heavy-ion induced stripping reactions on nuclear targets at $E_{\text{lab}} = 5 - 300$ MeV/nucleon, the in-medium effects lead to about 10% change in the nucleon knockout cross sections and momentum distributions. In (p, pN) processes, the in-medium effects are expected to be of the same order or smaller. The in-medium effects should decrease with increasing beam energy rendering Glauber model more natural at $E_{\text{lab}} > 1$ GeV/nucleon [14]. Thus, our description of ISI/FSI within Glauber model should

¹ It was pointed out in Ref. [20] that “the numerical differences in the results of calculations employing the “old” and “new” definitions are usually not large for single-nucleon channels, in contrast to cluster channels”. Thus, we do not expect much influence of this correction on our results.

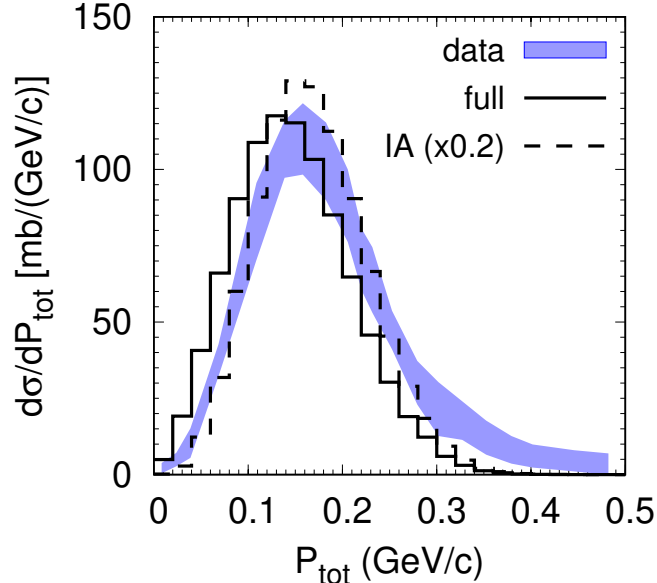


FIG. 6. The distribution of the total momentum of the residual nucleus in the r.f. of ^{12}C for $^{12}\text{C}(p, 2p)^{11}\text{B}$ at 400 MeV/nucleon. Line notations are the same as in Fig. 2. The band represents experimental data from Ref. [4].

be taken with some reservations for possible in-medium corrections.

5. SUMMARY

Based on the TISM, we developed the model for description of fully exclusive $A(p, pp)(A-1)$ reactions at intermediate relativistic energies. The model allows to calculate spectroscopic factors directly from the overlap integral of the WFs. Having in mind future model applications at NICA and FAIR energies, we restricted ourselves to the Glauber model description of the ISI/FSI. As a test case, the model was applied to the reaction $^{12}\text{C}(p, 2p)^{11}\text{B}$ at 400 MeV/nucleon measured at GSI [4] in the inverse kinematics.

The model slightly underestimates the measured integrated cross section for ^{11}B $3/2^-$ ground state, but overpredicts the integrated cross sections for the two excited $1/2^-$ and $3/2^-$ states. The total integrated cross section for the production of all three ^{11}B states is well reproduced, however.

The distributions of the outgoing proton pair in the opening angle and relative azimuthal

angle, as well as the momentum distributions of the residual nucleus, are reproduced reasonably well. Some deficiency in the production of high-momentum residual nuclei can be attributed to the longitudinal momenta mostly and is probably due to the limited HO WF basis.

Last but not least, the present calculation also puts on a firm ground our previous study of the $^{12}\text{C}(p, 2pN_s)^{10}\text{A}$ exclusive reactions at 48 GeV/c [6], where a similar approach has been used.

ACKNOWLEDGMENTS

The authors are grateful to Prof. Eliezer Piassetzky who proposed to apply for the $^{12}\text{C}(p, 2p)^{11}\text{B}$ reaction the same TISM setup as for the $^{12}\text{C}(p, 2pn_s)^{10}\text{B}$ reaction studied in Ref. [6].

-
- [1] Y. Kondo *et al.*, Phys. Rev. C **79**, 014602 (2009).
 - [2] M. Holl *et al.* (R3B), Phys. Lett. B **795**, 682 (2019).
 - [3] T. Aumann *et al.*, Prog. Part. Nucl. Phys. **118**, 103847 (2021), arXiv:2012.12553 [nucl-th].
 - [4] V. Panin *et al.*, Phys. Lett. B **753**, 204 (2016).
 - [5] V. G. Neudatchin and Y. F. Smirnov, *Nuklonnye assotsiatsii v legkikh yadrakh (Nucleon Associations in Light Nuclei)* (Nauka, Moscow, 1969) [in Russian].
 - [6] A. B. Larionov and Y. N. Uzikov, (2023), arXiv:2311.06042 [nucl-th].
 - [7] M. Patsyuk *et al.*, Nature Phys. **17**, 693 (2021), arXiv:2102.02626 [nucl-ex].
 - [8] V. Balashov, A. Boyarkina, and I. Rotter, Nucl. Phys. **59**, 417 (1964).
 - [9] A. N. Boyarkina, *Struktura yader 1p-obolochki (Structure of 1p-shell Nuclei)* (Moskovskij Gosudarstvennij Universitet (Moscow State University), Moscow, 1973) [in Russian].
 - [10] Y. F. Smirnov and Y. M. Tchuvil'sky, Phys. Rev. **C15**, 84 (1977).
 - [11] Y. Uzikov and A. Uvarov, Phys. Part. Nucl. **53**, 426 (2022).
 - [12] H. A. Jahn and H. van Wieringen, Proc. Roy. Soc. A **209**, 502 (1951).
 - [13] J. Elliott, J. Hope, and H. A. Jahn, Phil. Trans. Roy. Soc. **A246**, 241 (1953).
 - [14] B. Van Overmeire, W. Cosyn, P. Lava, and J. Ryckebusch, Phys. Rev. C **73**, 064603 (2006),

arXiv:nucl-th/0603013.

- [15] G. D. Alkhazov, G. M. Amalsky, S. L. Belostotsky, A. A. Vorobyov, O. A. Domchenkov, Y. V. Dotsenko, and V. E. Starodubsky, *Phys. Lett. B* **42**, 121 (1972).
- [16] J. Cugnon, J. Vandermeulen, and D. L'Hote, *Nucl. Instrum. Meth. B* **111**, 215 (1996).
- [17] S. Cohen and D. Kurath, *Nucl. Phys. A* **101**, 1 (1967).
- [18] R. N. Singh, N. De Takacsy, S. I. Hayakawa, R. L. Hutson, and J. J. Kraushaar, *Nucl. Phys. A* **205**, 97 (1973).
- [19] J. Li, C. A. Bertulani, and F. Xu, *Phys. Rev. C* **105**, 024613 (2022), arXiv:2202.04354 [nucl-th].
- [20] D. M. Rodkin and Y. M. Tchuvil'sky, *Phys. Rev. C* **104**, 044323 (2021), arXiv:2104.10499 [nucl-th].
- [21] D. W. Devins, D. L. Friesel, W. P. Jones, A. C. Attard, I. D. Svalbe, V. C. Officer, R. S. Henderson, B. M. Spicer, and G. G. Shute, *Aust. J. Phys.* **32**, 323 (1979).
- [22] T. Aumann, C. A. Bertulani, and J. Ryckebusch, *Phys. Rev. C* **88**, 064610 (2013), arXiv:1311.6734 [nucl-th].
- [23] C. A. Bertulani and C. De Conti, *Phys. Rev. C* **81**, 064603 (2010), arXiv:1004.2096 [nucl-th].